COMMUNICATION

Creating In-Plane Metallic-Nanowire Arrays by Corner-Mediated Electrodeposition

By *Bo Zhang, Yu-Yan Weng, Xiao-Ping Huang, Mu Wang,* Ru-Wen Peng, Nai-Ben Ming, Bingjie Yang, Nan Lu,* and *Lifeng Chi*

Metallic microstructures are the essential building blocks in microelectronics as electric interconnection between different functioning parts.[1] In the blooming field of optoelectronics, metallic microstructures also play a key role due to surface-plasmon-plariton-related effects,[2,3] applications in miniaturization of photonic circuits,[4,5] near-field optics,[6] and single-molecule optical sensing.[7,8] The electromagnetic resonance in metallic microstructures may offer unique properties that do not exist in natural materials, such as negative refractive index.[9,10] In previous studies, metallic microstructures were usually fabricated by photolithography, which was time-consuming and costly.[11] Template-assisted electrodeposition is an easy way to fabricate microstructures. For example, anodic aluminum oxide (AAO)[12–14] and polymeric membranes[15] have been used as molds, and the size of the channels in these systems can reach a few nanometers.[16] However, the destructivity in removal template renders it difficult to preserve the spatial order among the nanowires,[17,18] hence limits their applications in optoelectronics. We once introduced a selective electrodeposition method to fabricate two-dimensional metallic structures, where the substrate surface was modified by stripes of lipid monolayers, on which nucleation of metal crystallites was easier.[19] However, in that case the width of the metallic wires was limited by the geometrical shape of templates, that is, the width of metallic wires could not be tuned unless a new template was used. Furthermore, previously fabricated wires[19] were essentially flat belts lying on the substrate, which would not be effective if applied to sensors where a large specific surface area is usually expected.[20] Therefore, one of the important challenges in fabricating metallic microstructures is to find an easy, repeatable, and controllable method to meet the increasing demands in optoelectronics and plasmonics.

[*] Prof. M. Wang, B. Zhang, Dr. Y. Weng, X. Huang, Prof. R. W. Peng, Prof. N. B. Ming
National Laboratory of Solid State Microstructures
Department of Physics
Nanjing University
Nanjing 210093 (China)
E-mail: muwang@nju.edu.cn
B. Yang, Prof. N. Lu, Prof. L. Chi
Key Laboratory for Supramolecular Structure and Materials,
Jilin University
Changchun 130012 (China)
Prof. L. Chi
Physikalisches Institut and Center for Nanotechnology (CeNTech)
Westfälische Wilhelms-Universität
Münster D-48149 (Germany)

DOI: 10.1002/adma.200900730

In this communication, we report a new template-assisted electrochemical approach to fabricate arrays of metallic nanowires. Unlike conventional template-assisted growth, where the generated wires are confined by the size of template, in our case the width of the metallic wires can be tuned by changing the control parameters of electrodeposition. By imprinting polymer stripes on a silicon surface, the concave corner of polymer stripes and silicon substrate provides a preferential nucleation site for the formation of metal nanowires. The width of wires can be tuned from 25 nm to a few hundred nanometers. Further, we demonstrate that this method can be applied for fabricating more complicated structures rather than straight lines only.

In our experiments, the metallic nanowires are electrodeposited with the help of polymer stripes embossed on silicon surfaces. To form the patterned substrate, a thin film of poly(methylmethacrylate) (PMMA) (mr-I 7030E $M_w = 75$ kDa) is initially spin-coated on the silicon wafer. The film thickness is about 300 nm. The stripe patterns are introduced by nanoimprint lithography (NIL).[21] The pressure applied on mold and the temperature of embossing are carefully selected, so PMMA may flow into the cavities and reproduce the mold pattern. In our experiments, the pressure is 40 bar (1 bar $= 10^5$ Pa), and the embossing temperature is 170 °C. The entire system is thereafter cooled below the glass-transition temperature (T_g) before demolding. After conformal molding, the residual polymer on the bottom of trench is removed by oxygen reactive-ion etching (O-RIE). In this way, periodic stripes of PMMA are generated on the silicon surface. The schematic diagram for substrate preparation is shown in Figure 1a. The striped substrate before electrodeposition is shown in Figure 1b, where the darker stripe region is covered with PMMA, and the brighter area is the surface of silicon substrate. The height of the PMMA stripes is about 80 nm.

On a PMMA-striped silicon substrate, we carry out copper electrodeposition with our previously reported ultrathin electrochemical-deposition setup,[22–25] where copper nanowires grow in an ultrathin electrolyte layer of a few hundred nanometers thick. The schematic diagrams of the experimental setup are shown in Figure 1c. The concentration of aqueous electrolyte of $CuSO_4$ is 0.05 M (pH 4.5). Potentiostatic electrodeposition is carried out with a constant voltage in the range 0.2–1.5 V across the electrodes. We observe that copper prefers to nucleate at the edge of the PMMA stripe. Successive nucleation of copper eventually forms the array of straight, homogeneous copper wires, as shown in Figure 1d.

Our experimental observations show that the width of copper wires depends on both the concentration of electrolyte $CuSO_4$ and the electric voltage across the electrodes. Figure 2a–c provides the

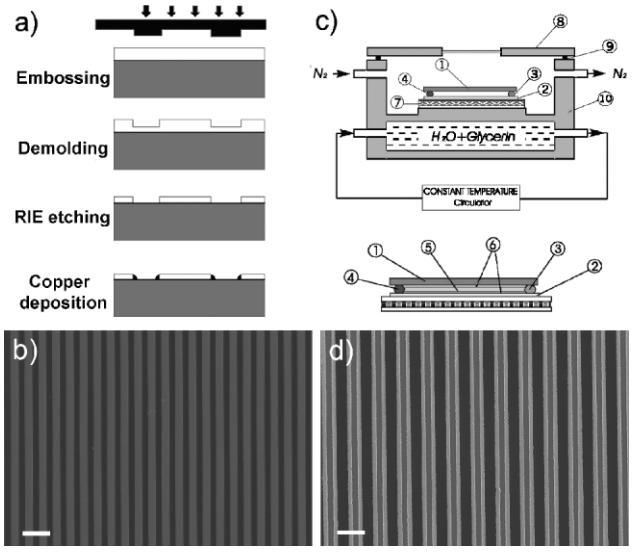

Figure 1. a) Schematic diagrams showing the procedures to prepare the PMMA-striped substrate. b) SEM image of the PMMA-striped silicon substrate. The area with the dark contrast is covered with PMMA. The scale bar represents 4 μm. c) Schematic diagrams of the electrodeposition setup with an ultrathin electrolyte layer by freezing the electrolyte solution. 1) Top glass plate; 2) bottom PMMA-striped silicon substrate; 3) cathode; 4) anode; 5) ice of electrolyte; 6) the ultrathin electrolyte layer trapped between the ice of electrolyte and the substrate; 7) Peltier element used for stimulating nucleation of electrolyte ice in freezing process; 8) top cover of the thermostated chamber with a glass window for optical observation; 9) rubber O-ring for sealing; 10) the thermostated chamber. d) SEM image of the copper-wire array generated on the PMMA-striped substrate. The lines with the brighter contrast are the copper wires, the lines with the darker contrast are the PMMA stripes, and the area with the gray contrast is the silicon substrate. The scale bar represents 2 μm.

morphology of copper wires fabricated at voltages varying from 0.6–0.3 V, where the line width changes from 110 to 25 nm. The length of the copper wires in our experiments can easily reach 0.5 cm, which in fact is determined by the separation of the electrodes. Figure 2d shows the dependence of wire width and electric voltage across the electrodes. It is clear that narrower copper wires can be achieved at lower voltage.

To verify the chemical purity of the metallic wires, mapping of energy-dispersive spectrometry (EDS) has been applied, as shown in Figure 3. In the selected scan region, the red lines are the imaging of copper element, and the green background is the imaging of silicon substrate. The EDS data do not show detectable concentration of oxygen along the wires. In fact, as we have reported earlier,[26] oxide of copper generated in electrodeposition can be efficiently avoided when electrodeposition is carried out in acidified solution.

In order to understand the growth mechanism of the copper nanowires along the edge of PMMA stripes, we check the detailed morphology of the very front tip of a wire, as shown in Figure 4a. It is clear that the wire develops at the concave corner of PMMA stripe and silicon substrate, and selective nucleation at the concave corner contributes to the wire growth. We expect that the width of the wires depends on the local nucleation rate. In fact, according to theory of crystallization, nucleation rate of Cu grains is exponentially related to the driving force of

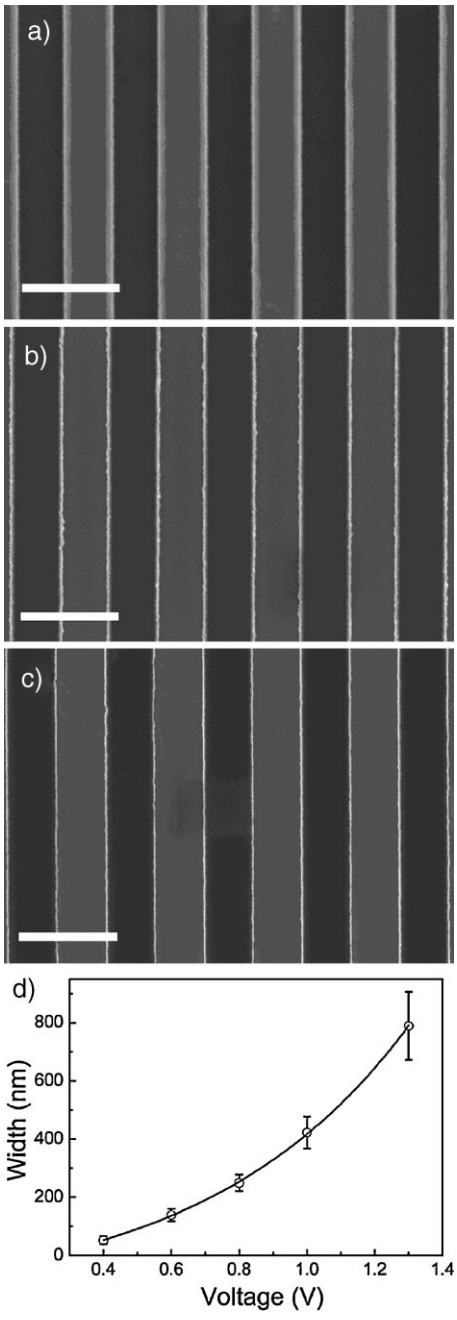

Figure 2. a–c) SEM images of the copper-nanowire array generated at different applied voltages in electrodeposition. The scale bar represents 2 μm. a) $V = 0.6$ V. b) $V = 0.4$ V. c) $V = 0.3$ V. d) The dependence of the line width of the copper wires as a function of the applied voltage across the electrodes.

electrocrystallization (overpotential).[27] One may actually find from Figure 2d that the width of the wires increases more rapidly when the applied voltage is high, which is consistent with the nucleation theory. The distance between neighboring metallic nanowires, however, is determined by the template, that is, by the separation between the stripes and the width of PMMA stripe itself.

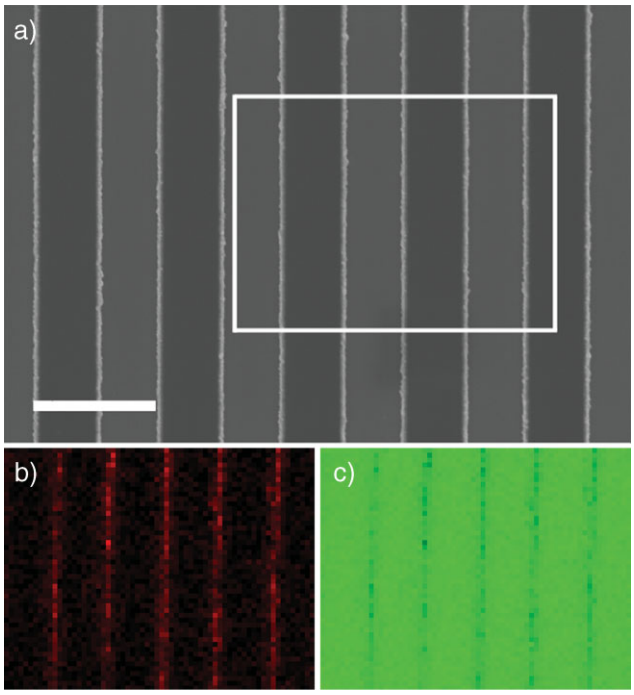

Figure 3. Mapping of the EDS was carried out in the selected area. The electric voltage to deposit this sample was 0.45 V and pH of electrolyte was 4.5. The bottom-left graph shows the imaging for copper element (red lines); the bottom-right graph shows the imaging for silicon, where the areas covered with copper wires are darkened. The scale bar represents 2 μm.

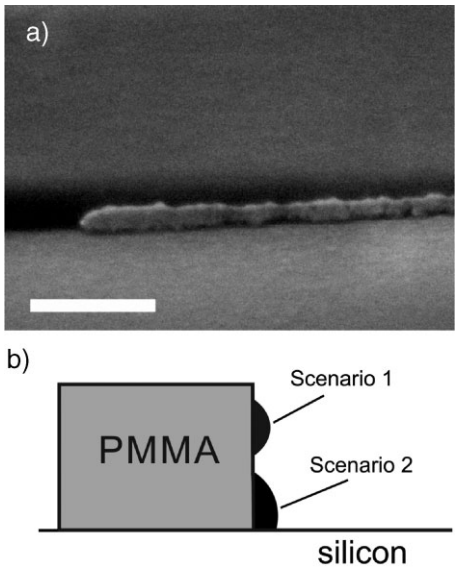

Figure 4. a) SEM image of the concave-corner region of the PMMA stripe and the silicon substrate. The tip of a copper nanowire can be clearly identified. The sample has been tilted 70° for imaging. The scale bar represents 200 nm. b) Schematic diagram showing the possible sites of nucleation in electrodeposition. For Scenario 1, copper nucleus contacts the PMMA surface only. For Scenario 2, copper nucleus appears at the concave corner, and contacts both the PMMA stripe and the silicon substrate.

Thermodynamically, the growth process of the copper wires can be understood as follows. As illustrated in Figure 1c and 4b, the electrolyte layer trapped between the substrate and the electrolyte ice is very thin. Therefore, nutrient transfer to the top surface of PMMA stripes is severely confined. Consequently, nucleation and crystallization of copper on the top surface of the PMMA stripe is restricted. This feature distinguishes our work with that in ref. [19]. The key factor that governs the growth behavior is the difference of the energy barrier for nucleation on the side face of PMMA stripe (Scenario 1) and that along the concave corner of PMMA stripe and silicon substrate (Scenario 2, Fig. 4b). In Scenario 1, the embryo of nucleus initiates on PMMA surface, and we assume that the embryo keeps a shape of spherical cap. For Scenario 2, the substrate is asymmetric: on one side, the substrate is the PMMA stripe, whereas on the other side, the substrate is silicon covered with a very thin layer of oxide. Based on thermodynamics, one may find that the energy barrier for nucleation in Scenario 1[26,27] is

$$\Delta G_1^* = \frac{8r_{cf}^2\Omega_c}{\Delta g}(\theta_1 - \cos\theta_1 \sin\theta_1), \quad (1)$$

where θ_1 is the contact angle of the copper nucleus and the PMMA surface, Δg is the change of the free energy required for a copper ion to become a copper atom in electrocrystallization, and Ω_c is the volume of a copper atom. The interfacial energy of the copper nucleus and the electrolyte is denoted as r_{cf}. Once this energy barrier is overcome, the nucleus will spontaneously grow up. The energy barrier for nucleation in Scenario 2 can be written as

$$\Delta G_2^* = \frac{8r_{cf}^2\Omega_c}{\Delta g} \times \frac{[\theta_1 + \theta_2 - \pi/2 - (\sin\theta_1 - \cos\theta_2)\cos\theta_1 - (\sin\theta_2 - \cos\theta_1)\cos\theta_2]}{2} \quad (2)$$

where θ_2 is the contact angle of a copper nucleus and surface of silicon substrate. It follows that the difference between these two energy barriers, δ, can be expressed as

$$\delta = \Delta G_1^* - \Delta G_2^* = \frac{8r_{cf}^2\Omega_c}{\Delta g}[\pi/4 - \cos\theta_1\cos\theta_2 + \theta_1/2 - \cos\theta_1\sin\theta_1/2 + \sin\theta_2\cos\theta_2/2 - \theta_2/2] \quad (3)$$

It is the sign of δ that decides the energetically favorable sites for nucleation. It has been experimentally observed that copper crystallites deposit easily on PMMA surfaces, while nucleation on

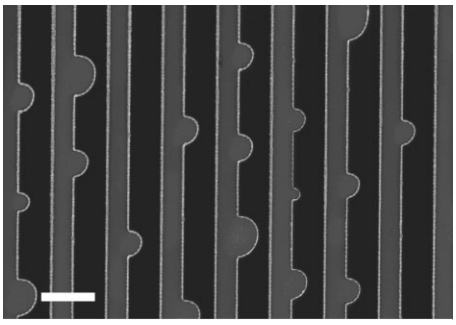

Figure 5. In preparation of the arrays of PMMA strips (the dark stripes in the picture) on silicon substrate, some hemicycle defects are occasionally generated. This SEM image shows that the copper wires may follow the edge of the PMMA stripes in electrodeposition and develop into a more complicated pattern. The scale bar represents 2 μm.

the surface of silicon substrate is more difficult.[12,28] This suggests that θ_1 should be less than $\frac{\pi}{2}$ and θ_2 is larger than $\frac{\pi}{2}$, although we do not know the exact value of these data. By taking the estimated value of θ_1 and θ_2 into the expression of δ, one may find that δ is positive in this regime. This means that nucleation at the concave corner (Scenario 2) is indeed favorable in electrodeposition.

The unique electrodeposition behavior reported here demonstrates a simple and controllable way to fabricate in-plane arrays of long, straight copper nanowires on a solid substrate. According to the corner-mediated mechanism discussed above, this method should also be applicable for fabricating structures beyond straight-line array when patterned PMMA structures are introduced. In fact, in nanoimprinting process, some hemicycle defects occasionally occur on the edge of the PMMA stripes. We find that copper nucleation may follow the edge of PMMA stripes and sketch out the profile of the stripes, as shown in Figure 5. This observation suggests that if PMMA stripes possess a more complicated topography, it is possible to fabricate irregular metallic structures that mimic the outline of the stripe edges. This feature becomes especially interesting nowadays, because of recent intensive investigations in fabricating sub-wavelength metallic structures with the aim to construct metamaterials.[9,10,29–32] Our observations demonstrate the possibility to fabricate sub-wavelength metallic structures in a more economical way.

In conventional template-assisted growth, the generated metal structures are usually the cast of template, where the wire is the cast of that of the template. In this paper, we introduce slightly higher PMMA stripes as template. The lower nucleation barrier at the concave corner of the PMMA stripe and the silicon substrate helps to nucleate the copper wire, and wire width can be tuned by controlling the local nucleation rate via the applied electric voltage. As illustrated in Figure 2, at lower voltage the copper wire can be as narrow as 25 nm. On the substrate, once the local nucleation barrier is lower at the concave corner, the unique growth behavior, as we have reported above, will occur. From this point of view, we anticipate that more complicated metallic patterns can be fabricated with our concave-corner-mediated electrodeposition, so do the wire arrays of other metals.

Experimental

Preparation of Striped Template: The original silicon master of linear gratings for nanoimprinting was fabricated by photolithography, followed by an anisotropic etching. To prepare the striped substrate for electrodeposition in this experiment, a 100-orientated silicon wafer was cleaned and oxidized by oxygen plasma (PVA Tepla System 100-E). A thin film of PMMA (mr-I 7030E, $M_w = 75$ kDa) was then spin-coated on the silicon substrate, and baked on a hot plate for 5 min at 130 °C. The film thickness was controlled to 300 nm. A 2.5-inch nanoimprinter (Obducat AB, Sweden) was used, and the stamps were imprinted into the PMMA film for 5 min under a pressure of 40 bar. The embossing temperature was 170 °C. The entire system was thereafter cooled below the glass-transition temperature (T_g) before demolding. After conformal molding, the residual PMMA on the bottom of the embossed structures was removed by oxygen reactive-ion etching. The PMMA-striped substrate was used for electrodeposition without further cleaning.

Copper Electrodeposition: The electrodeposition was carried out in a system consisting of two parallel, straight electrodes made of copper foil 100 μm in thickness (99.9% pure, Goodfellow). The separation of the electrodes is fixed as 1.0 cm. The electrodes were bound by two rigid boundaries, one of which was the silicon wafer covered with PMMA stripes, and the other was a conventional glass microscope slice. The PMMA stripes were arranged perpendicular to the linear cathode and the anode. So the copper wires initiated from the cathode, followed the edges of the stripes, and developed toward the anode.

The electrolyte solution for electrochemical deposition was prepared by analytical regent $CuSO_4$ and deionized, ultrapure water (Millipore, electric resistivity 18.2 $M\Omega^{-1}$cm). The initial concentration of $CuSO_4$ aqueous electrolyte was 0.05 M, and pH was 4.5. In order to generate the ultrathin electrolyte layer for electrodeposition, a constant-temperature circulator (Polystat 12108-35, Cole Parmer) and a Peltier element were used to decrease the temperature of electrodeposition cell and to solidify the electrolyte (as shown in Fig. 1b). Detailed description of the electrodeposition system can be found in refs. [22–25]. Dry nitrogen gas flowed through the electrodeposition chamber to prevent water condensation on the glass window, so in situ optical observation could be applied to monitor the solidification processes of the electrolyte and the electrodeposition process. The temperature of the electrodeposition cell was decreased to −4 °C by the programmable thermostat.

During the solidification process, part of the salt in aqueous electrolyte was expelled from the ice due to partitioning effect [33–35], hence the electrolyte concentration became gradually higher. When equilibrium was eventually reached at the set temperature (−4 °C, for example), an ultrathin layer of concentrated electrolyte remained unsolidified between the ice of electrolyte and the patterned silicon substrate. The thickness of this ultrathin layer depended on temperature, initial concentration of electrolyte, and amount of electrolyte solution in the deposition cell [23,36]. In our system, the typical thickness of this layer was of the order of several hundreds of nanometers. In this ultrathin electrolyte layer the array of copper nanowires was electrodeposited. In order to get a flat interface of ice of electrolyte, repeated solidification, and melting was applied with the help of Peltier element, until only one or just a few nuclei of ice remained in the deposition cell. The temperature-decreasing rate in solidifying the electrolyte was kept as low as about 0.1 °C h^{-1} in order to resume the flat interface of ice/electrolyte. Potentiostatic electrodeposition was applied and a constant electric voltage was set in the range of 0.2–1.5 V. The copper filaments firmly sticked at the concave corner of the PMMA stripe and silicon substrate. After electrodeposition, copper electrodeposits were rinsed with ultrapure water and dried in a vacuum chamber for further analyses. A field-emission scanning electron microscope (LEO 1530VP) was used to analyzed the copper-nanowire arrays.

Acknowledgements

This work has been funded by the Ministry of Science and Technology of China (2004CB619005 and 2006CB921804), the National Science

Foundation of China (10625417 and 10874068) and Jiangsu province (BK2008012).

Received: March 2, 2009
Revised: March 5, 2009
Published online: May 12, 2009

[1] S. Luryi, J. Xu, A. Zaslavsky, *Future Trends in Microelectronics: The Nano Millennium*, Wiley-Interscience, New York **2002**.
[2] T. W. Ebbesen, H. J. Lezec, H. F. Ghaemi, T. Thio, P. A. Wolff, *Nature* **1998**, *391*, 667.
[3] J. B. Pendry, L. Martin-Moreno, F. J. Garcia-Vidal, *Science* **2004**, *305*, 847.
[4] W. L. Barnes, A. Dereux, T. W. Ebbesen, *Nature* **2003**, *424*, 824.
[5] E. Ozbay, *Science* **2006**, *311*, 189.
[6] C. Girard, *Rep. Prog. Phys.* **2005**, *68*, 1883.
[7] S. M. Nie, S. R. Emery, *Science* **1997**, *275*, 1102.
[8] K. Kneipp, Y. Wang, H. Kneipp, L. T. Perelman, I. Itzkan, R. R. Dasari, M. S. Feld, *Phys. Rev. Lett.* **1997**, *78*, 1667.
[9] V. G. Veselago, *Sov. Phys. Usp.* **1968**, *10*, 509.
[10] R. A. Shelby, D. R. Simth, S. Schultz, *Science* **2001**, *293*, 77.
[11] B. Fay, *Microelectron. Eng.* **2002**, *61*, 11.
[12] T. M. Whitney, J. S. Jiang, P. C. Searson, C. L. Chien, *Science* **1993**, *261*, 1316.
[13] a) X. Y. Zhang, L. D. Zhang, G. W. Meng, G. H. Li, N. Y. Jin-Philipp, F. Philipp, *Adv. Mater.* **2001**, *13*, 1238; b) Y. T. Pang, G. W. Meng, L. D. Zhang, Y. Qin, X. Y. Gao, A. W. Zhao, Q. Fang, *Adv. Funct. Mater.* **2002**, *12*, 719.
[14] A. H. Liu, M. Ichihara, I. Honma, H. S. Zhou, *Electrochem. Comm.* **2007**, *9*, 1766.
[15] C. R. Martin, *Science* **1994**, *266*, 1994.
[16] B. H. Hong, S. C. Bae, C. W. Lee, S. Jeong, K. S. Kim, *Science* **2001**, *294*, 348.
[17] Z. Zhang, D. Gekhtman, M. S. Dresselhaus, J. Y. Ying, *Chem. Mater.* **1999**, *11*, 1659.
[18] W. Yoo, J. Lee, *Adv. Mater.* **2004**, *16*, 1097.
[19] M. Z. Zhang, S. Lenhert, M. Wang, L. F. Chi, N. Lu, H. Fuchs, N. B. Ming, *Adv. Mater.* **2004**, *16*, 409.
[20] Z. M. Qi, I. Honma, H. S. Zhou, *Appl. Phys. Lett.* **2007**, *90*, 011102.
[21] a) S. Y. Chou, P. R. Krauss, P. J. Renstrom, *Appl. Phys. Lett.* **1995**, *67*, 3114. b) S. Y. Chou, P. R. Krauss, P. J. Renstrom, *Science* **1996**, *272*, 85.
[22] M. Wang, S. Zhong, X. B. Yin, J. M. Zhu, R. W. Peng, N. B. Ming, *Phy. Rev. Lett.* **2001**, *86*, 3827.
[23] S. Zhong, Y. Wang, M. Wang, M. Z. Zhang, X. B. Yin, R. W. Peng, N. B. Ming, *Phys. Rev. E* **2003**, *67*, 061601.
[24] Y. Wang, Y. Cao, M. Wang, S. Zhong, M. Z. Zhang, Y. Feng, R. W. Peng, X. P. Hao, N. B. Ming, *Phys. Rev. E* **2004**, *69*, 021607.
[25] T. Liu, S. Wang, Z. L. Shi, G. B. Ma, M. Wang, R. W. Peng, X. P. Hao, N. B. Ming, *Phys. Rev. E* **2007**, *75*, 051606.
[26] M. Z. Zhang, Y. Wang, G. W. Yu, M. Wang, R. W. Peng, N. B. Ming, *J. Phys.: Condens. Matter* **2004**, *16*, 695.
[27] I. V. Markov, *Crystal Growth for Beginners: Fundamentals of Nucleation, Crystal Growth and Epitaxy*, 2nd ed., World Scientific, Singapore **2003**.
[28] A. Zangwill, *Physics at Surfaces*, Cambridge University Press, Cambridge, U.K **1988**.
[29] D. R. Smith, J. B. Pendry, M. C. K. Wiltshire, *Science* **2004**, *305*, 788.
[30] N. Fang, H. Lee, C. Sun, X. Zhang, *Science* **2005**, *308*, 534.
[31] K. L. Tsakmakidis, A. D. Boardman, O. Hess, *Nature* **2007**, *450*, 397.
[32] X. Zhang, Z. Liu, *Nat. Mater.* **2008**, *7*, 436.
[33] N. B. Ming, *Fundamentals of Crystal Growth Physics*, Shanghai Science and Technology, Shanghai **1982**.
[34] W. Kurz, D. J. Fisher, *Fundamentals of Solidification*, 4th ed., Enfield Publishing & Distribution Company, Enfield, NH **2001**.
[35] A. Pimpinelli, J. Villain, *Physics of Crystal Growth*, Cambridge University Press, Cambridge **1998**.
[36] Y. Y. Weng, J. W. Si, W. T. Gao, Z. Wu, M. Wang, R. W. Peng, N. B. Ming, *Phys. Rev. E* **2006**, *73*, 051601.